Rapid Communications

Low-momentum dynamic structure factor of a strongly interacting Fermi gas at finite temperature: The Goldstone phonon and its Landau damping

Peng Zou,[1] Hui Hu,[2] and Xia-Ji Liu[2]

[1]*College of Physics, Qingdao University, Qingdao 266071, China*

[2]*Centre for Quantum and Optical Science, Swinburne University of Technology, Melbourne, Victoria 3122, Australia*

(Received 22 December 2017; published 16 July 2018)

We develop a microscopic theory of the dynamic structure factor to describe the Bogoliubov-Anderson-Goldstone phonon mode and its damping rate in a strongly interacting Fermi gas at finite temperature. It is based on a density functional approach—the so-called superfluid local density approximation. The accuracy of the theory is quantitatively examined by comparing the theoretical predictions with recent experimental measurements for the local dynamic structure factor of a nearly homogeneous unitary Fermi gas at low transferred momentum [S. Hoinka *et al.*, Nat. Phys. **13**, 943 (2017)], without any free parameters. We calculate the dynamic structure factor as functions of temperature and transferred momentum, and determine the temperature evolution of the phonon damping rate, by considering the dominant decay process of the phonon mode via scatterings off fermionic quasiparticles. These predictions can be confronted with future Bragg scattering experiments on a unitary Fermi gas near the superfluid transition.

DOI: 10.1103/PhysRevA.98.011602

Introduction. The understanding of the density fluctuation spectrum of superfluid ^{4}He plays a central role in the early development of quantum many-body physics [1,2]. The modern concept of quasiparticles began with Landau's original theory of superfluid ^{4}He [3]. The extensive studies of either Brillouin and Raman light scattering [4] or inelastic neutron scattering [2] in such systems led to the discovery of phonons and rotons. In particular, the measurements of the sound attenuation reveal the underlying decay mechanism of quasiparticles. At low temperatures (i.e., $T \lesssim 0.6\,\mathrm{K} \sim 0.3T_c^{\mathrm{He}}$) in the collisionless regime, the decay rate of phonons Γ is due to the three-phonon Landau-Beliaev process and exhibits a characteristic ωT^4 dependence on the phonon frequency ω [4]. At higher temperatures ($T \gtrsim 1.0\,\mathrm{K} \sim 0.5T_c^{\mathrm{He}}$), superfluid ^{4}He crosses over to the hydrodynamic regime and the damping rate of phonons instead shows a quadratic ω^2 dependence [3].

After nearly 50 years, the community of quantum physics welcomes the arrival of another strongly interacting many-body system [5], a unitary Fermi gas at the cusp of the crossover from Bose-Einstein condensates (BECs) to Bardeen-Cooper-Schrieffer (BCS) superfluids [6]. This novel fermionic superfluid is unique, owing to the unprecedented accuracy in tuning almost all the controlling parameters of the system [7]. To date, there are already a number of milestone observations of a unitary Fermi gas, confirming its high-temperature superfluidity [8], measuring the zero-temperature equation of state [9], revealing the universal thermodynamics [10–13], and probing the second sound [14]. The density fluctuation spectrum is also measured, however, restricted to collective oscillations with *discrete* frequencies [15–19], due to the very existence of a harmonic trapping potential that is necessary to hold atoms from escaping. Only most recently, the density excitation spectrum of a nearly *homogeneous* unitary Fermi gas has been obtained at Swinburne University of Technology, by applying the low-momentum two-photon Bragg spectroscopy to determine the local dynamic structure factor near the trap center [20]. The purpose of this Rapid Communication is to present a microscopic theory that *quantitatively* explains the observed Bogoliubov-Anderson-Goldstone phonon mode and to provide reliable theoretical predictions on the phonon damping for future experimental confirmation.

The development of a quantitative description of the density response of a strongly interacting Fermi superfluid is by no means an easy task [21–30]. There is no small parameter to control the precision of the theory due to the divergent scattering length a_s in the unitary limit [6]. For the experimental work at Swinburne, the data have been qualitatively understood using a standard random-phase-approximation (RPA) theory, with a modified chemical potential as a fitting parameter [20]. The calculated spectrum overestimates the phonon peak (i.e., more than twice in height) and accounts for only two-thirds the measured width. This good but somewhat unsatisfactory agreement is partly because of the violation in the f-sum rule, as a result of the large modification to the mean-field chemical potential [20]. The quantitative agreement between our microscopic theory and experiment without any adjustable parameters, as found in this Rapid Communication, is therefore highly nontrivial.

The establishment of an accurate density response theory also allows us to identify the main decay mechanism for Goldstone phonons. In contrast to the three-phonon Landau-Beliaev processes as previously suggested [31], we clarify that the phonon damping is dominated by the inelastic process of absorption or emission by fermionic quasiparticles [32–34]. We determine the inverse quality factor Γ/ω of a unitary Fermi gas as functions of temperature and transferred momentum. These predictions could be readily examined in state-of-art experiments in cold-atom laboratories.

Density response theory within SLDA. We start by briefly reviewing the superfluid local density approximation (SLDA) of

a unitary Fermi gas [35,36] and the resulting improved SLDA-RPA theory for density response functions [29]. As the s-wave scattering length a_s diverges in the unitary limit, the low-energy physics of the system can be well governed by a regularized energy density functional $\mathcal{E}[\tau_c(\mathbf{r},t), n(\mathbf{r},t), \nu_c(\mathbf{r},t)]$,

$$\mathcal{E}[\tau_c, n, \nu_c] = \frac{\tau_c}{2m} + \beta\frac{3(3\pi^2)^{2/3}}{10m}n^{5/3} + g_{\rm eff}|\nu_c|^2, \quad (1)$$

where $\tau_c = 2\sum_{|\mathbf{k}|<\Lambda}|\nabla v_{\mathbf{k}}|^2$ is the kinetic density, $n = 2\sum_{|\mathbf{k}|<\Lambda}|v_{\mathbf{k}}|^2$ the number density, $\nu_c = \sum_{|\mathbf{k}|<\Lambda}u_{\mathbf{k}}v_{\mathbf{k}}^*$ the anomalous Cooper-pair density, $u_{\mathbf{k}}(\mathbf{r},t)$ and $v_{\mathbf{k}}(\mathbf{r},t)$ are the Bogoliubov quasiparticle wave functions, to be determined by solving a generalized Bogoliubov–de Gennes equation for momentum $\mathbf{k}$ below the cutoff momentum Λ [29,35–37], and $g_{\rm eff}^{-1} \equiv mn^{1/3}/\gamma - \sum_{|\mathbf{k}|<\Lambda} m/\mathbf{k}^2$ is the inverse effective coupling constant. The form of the above energy density functional is the most general form allowed by the scale invariance, which is satisfied at unitarity. The two *temperature-independent* parameters β and γ can be uniquely fixed by requiring that the resulting chemical potential μ and pairing gap Δ agree with those calculated by microscopic theories or measured experimentally [38]. As the pairing gap is related to the anomalous density ν_c by $\Delta(\mathbf{r},t) = -g_{\rm eff}\nu_c(\mathbf{r},t)$, we may rewrite the interaction part of the density functional as

$$\mathcal{E}_{\rm int} = \beta\frac{3(3\pi^2)^{2/3}}{10m}[n(\mathbf{r},t)]^{5/3} + \frac{|\Delta(\mathbf{r},t)|^2}{g_{\rm eff}}. \quad (2)$$

Let us consider the fluctuations in the number densities $n_\uparrow(\mathbf{r},t)$, $n_\downarrow(\mathbf{r},t)$, and Cooper-pair density $\nu_c(\mathbf{r},t)$ and its complex conjugate $\nu_c^*(\mathbf{r},t)$, to be collectively denoted as δn_i or δn_j ($i, j = \uparrow, \downarrow, c, c^*$). Here, we have split the total density $n(\mathbf{r},t)$ into the spin-up and spin-down components to allow the calculation of spin-density dynamic structure factor. These local fluctuations induce a self-generated mean-field potential $\sum_j E_{ij}^I \delta n_j$, where $E_{ij}^I = (\delta^2\mathcal{E}_{\rm int}/\delta n_i \delta n_j)$ [21,23]. As a result, the dynamical response function takes the standard RPA form, $\chi = \chi^0[1-\chi^0 E^I]^{-1}$, where χ^0 is the bare response function without the inclusion of the induced potential [21]. The density response function is a summation of χ_{ij} in the density channel, i.e., $\chi_{nn}(\mathbf{k}, \omega + i0^+) = \chi_{11} + \chi_{12} + \chi_{21} + \chi_{22} = 2(\chi_{11} + \chi_{12})$. The dynamic structure factor is given by the imaginary part of χ_{nn}, i.e., $S(\mathbf{k},\omega) = -{\rm Im}\,\chi_{nn}/[\pi(1 - e^{-\hbar\omega/k_BT})]$.

In our previous work [29], we have derived the expression for the matrix E^I and calculated the dynamic and static structure factor at *zero* temperature. We have found that the SLDA-RPA dynamic structure factor satisfies the important f-sum rule and compressibility sum rule and the static structure factor $S(k)$ agrees very well with the latest quantum Monte Carlo result for $k < k_F$ [39], where k_F is the Fermi wave vector. The excellent agreement strongly indicates that our SLDA-RPA theory could be quantitatively reliable near the unitary limit at low temperature. Here, we confirm this anticipation by the more stringent comparison with the recent experimental measurements at *finite* but low temperature [20], without any free parameters.

Quantitative comparison. To foster the comparison, it should be noted that the experimentally measured density fluctuation spectrum includes *instrumental* broadening due to the finite duration of the Bragg pulse. It can be viewed as the intrinsic response function convoluted with a sinc line shape [42,43],

$${\rm Im}\,\chi_{nn}^{\rm (Br)}(\mathbf{k},\omega) = \int_{-\infty}^{\infty}d\omega'\frac{{\rm Im}\,\chi_{nn}(\mathbf{k},\omega')}{\pi\sigma_B}{\rm sinc}^2\left[\frac{\omega-\omega'}{\sigma_B}\right], \quad (3)$$

where ${\rm sinc}(x) \equiv \sin(x)/x$ and the energy resolution $\sigma_B = 2/\tau_{\rm Br}$ is set by the pulse duration ($\tau_{\rm Br} \simeq 1.2$ ms [20]). In addition, the experimental spectrum also includes broadening arising from the slight density inhomogeneity near the trap center ($\delta n/n \sim 0.08$) [20]. As the Fermi energy $\varepsilon_F \propto n^{2/3}$ at unitarity, we estimate the variation $\delta\varepsilon_F \simeq 0.06\varepsilon_F$. We account for this trap-induced broadening by further convoluting the spectrum with a Lorentzian line shape,

$${\rm Im}\,\chi_{nn}^{\rm (exp)}(\mathbf{k},\omega) = \int_{-\infty}^{\infty}d\omega'\frac{(\sigma_T/\pi){\rm Im}\,\chi_{nn}^{\rm (Br)}(\mathbf{k},\omega')}{[(\omega-\omega')^2+\sigma_T^2]}, \quad (4)$$

where $2\sigma_T = \delta\varepsilon_F$ is the full width at half maximum.

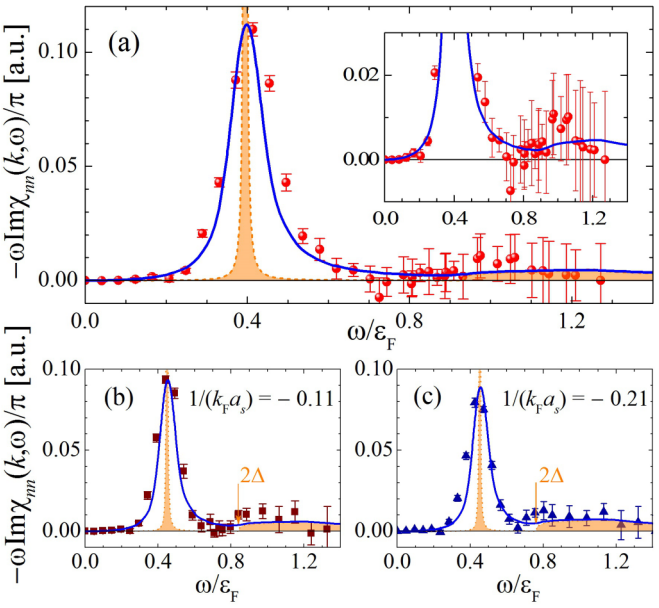

FIG. 1. The comparison between the SLDA-RPA theoretical predictions and the experimental data for $-\omega\,{\rm Im}\,\chi_{nn}(k,\omega)/\pi \equiv \omega(1-e^{-\hbar\omega/k_BT})S(k,\omega)$ at three sets of experimental conditions [20]: (a) the unitary limit with $1/(k_Fa_s) = 0$, $T = 0.09T_F$, and $k = 0.55k_F$, (b) $1/(k_Fa_s) = -0.11$, $T = 0.082T_F$, and $k = 0.60k_F$, and (c) $1/(k_Fa_s) = -0.21$, $T = 0.078T_F$, and $k = 0.59k_F$. The blue solid lines take into account the spectral broadening due to the finite duration of the Bragg pulse and due to the slight density inhomogeneity around the trap center (see text for more details), while the orange dotted lines with a shadow report the original SLDA-RPA results before the convolutions with the spectral broadening functions. The inset in (a) highlights the comparison near the pair-breaking excitations. In (b) and (c), the pair-breaking energy 2Δ is explicitly indicated by an arrow. The theoretical predictions are normalized to have the same area as the experimental results, according to the f-sum rule $-\int_0^\infty \omega\,{\rm Im}\,\chi_{nn}(k,\omega)/\pi d\omega = k^2/(2m)$. We have checked the f-sum rule in the SLDA-RPA theory at both zero temperature [29] and finite temperature. The satisfaction of the f-sum rule in the experimental measurement was previously used to confirm the universal relation for the static structure factor [40,41].

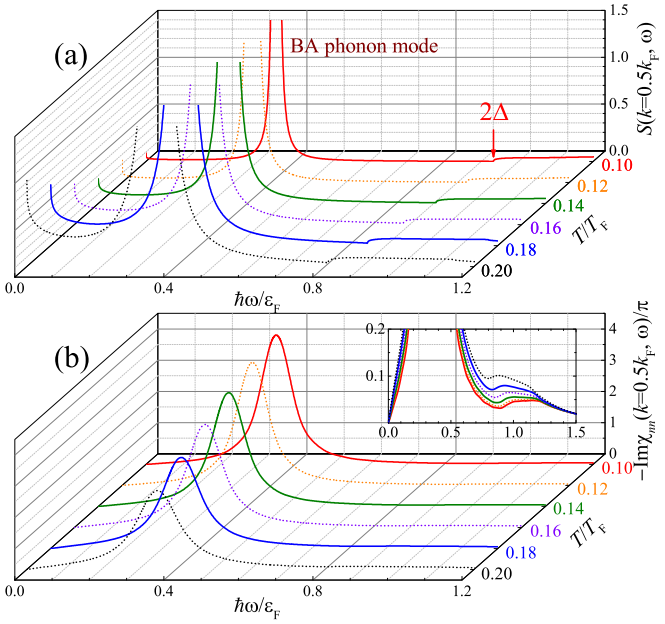

FIG. 2. Temperature evolution of the dynamic structure factor of a unitary Fermi gas at the transferred momentum $k = 0.5k_F$: (a) The original SLDA-RPA results $S(k, \omega)$ and (b) the more experimentally relevant predictions $-\mathrm{Im}\,\chi_{nn}(k, \omega)/\pi \equiv (1 - e^{-\hbar\omega/k_BT})S(k, \omega)$, after convolutions with the spectral broadening functions. The inset in the lower panel highlights the density response near the pair-breaking threshold 2Δ.

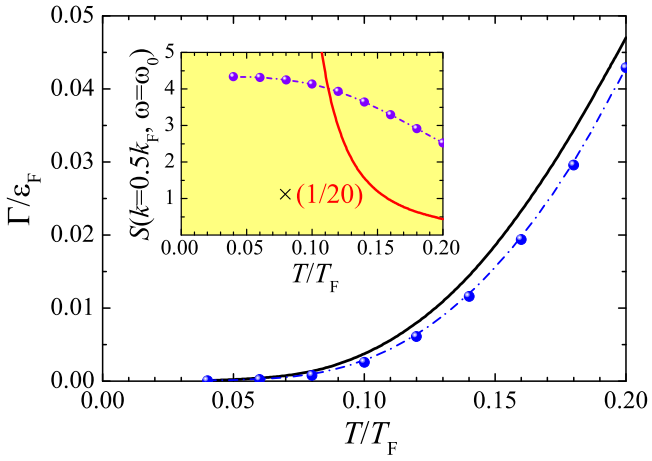

FIG. 3. The damping width of the Goldstone mode of a unitary Fermi gas at $k = 0.5k_F$, as a function of temperature. The black solid line shows the original SLDA-RPA results. The blue dotted-dashed line with circles reports $\delta\Gamma = \Gamma - \Gamma_0$, where $\Gamma(T)$ is obtained by convoluting the SLDA-RPA dynamic structure factor with the spectral broadening functions and $\Gamma_0 = \Gamma(T \to 0) \simeq 0.1\epsilon_F$ is the background width of the spectral broadening. The inset shows the dynamic structure factor at the peak position ω_0, without (red line) or with convolutions (purple dotted-dashed line with circles). For better illustration, the original SLDA-RPA result (red line) has been reduced by a factor of 20.

Figure 1 presents the comparison between the experimental spectra (symbols) and theoretical predictions obtained after performing the two convolutions (solid lines) [44], for three sets of parameters. We have used the zero-temperature equations of state given by a Gaussian pair fluctuation theory [45] as the inputs to determine the parameters β and γ at different interaction strengths [29]. At unitarity, this leads to $\beta \simeq -0.431$ and $1/\gamma \simeq -0.091$ [46]. The results for the density response function before the convolutions are also shown by dashed lines with a shadow. There is an excellent agreement for the *entire* spectrum, both at the unitary limit [Fig. 1(a)] and near unitarity [Figs. 1(b) and 1(c)]. Our theory greatly improves the previous RPA explanation [20], in the sense that (i) it removes the necessity of introducing a fitting parameter, to fit the measured peak position $\omega_0(k)$ of the Goldstone phonon mode; (ii) it fully accounts for the observed width and height of the peak; and (iii) it does not need to scale, in order to match the amplitude of the measured pair-breaking excitations at $\omega \sim 2\Delta$. The last point is particularly clear in Fig. 1, as the broad single-particle excitations are essentially unaffected by the instrumental broadening and trap inhomogeneity. The agreement is therefore highly nontrivial and actually it emphasizes the importance of the significant renormalization of single-particle behavior, due to the strong pairing effect, which is indeed taken into account in our theory via a density functional approach.

T dependence of the Goldstone mode. By establishing the reliability of our SLDA-RPA theory, we turn to consider the temperature evolution of the dynamic structure factor in the unitary limit, as shown in Fig. 2(a). The experimentally measurable density response (after convolutions) is reported in Fig. 2(b). Here and in the following, we have taken the experimentally determined chemical potential $\mu = 0.376\varepsilon_F$ [13] and pairing gap $\Delta = 0.47\varepsilon_F$ [20] to fix the parameters β and γ [46]. As temperature increases, it is apparent that the phonon peak in the spectrum becomes wider and lower, suggesting that the intrinsic width of the phonon mode becomes significant. Moreover, the single-particle excitations at around $\omega = 2\Delta$ are enhanced [see the inset in Fig. 2(b)]. Focusing on the Goldstone mode, we present the temperature dependence of its width and peak height in Fig. 3. It is interesting that, by subtracting a background width $\Gamma_0 \sim 0.1\varepsilon_F$ due to the instrumental and inhomogeneity broadenings, the width to be experimentally measured (symbols with a dotted-dashed line) is roughly equal to the *intrinsic* width of the phonon peak in the dynamic structure factor (solid line). This simply indicates that the intrinsic width of the Goldstone mode could be directly read from the measured width, with reasonable accuracy.

Landau damping. We now turn to discuss the intrinsic width or damping rate of the Goldstone phonon mode in greater detail. In Bose gases and Bose-Fermi mixtures, the Landau damping of phonons has been extensively studied [47–49]. In our case, what is the main mechanism responsible for damping? Physically, there are three possible sources that we may consider: (1) the three-phonon Landau-Beliaev process $\phi \longleftrightarrow \phi\phi$, where ϕ is the annihilation field operator of phonons; (2) the four-phonon Landau-Khalatnikov process $\phi\phi \longleftrightarrow \phi\phi$; and (3) the inelastic process of absorption or emission by the single-particle excitations. All these processes are responsible in the case of superfluid ^{4}He. For example, at low temperatures the three-phonon process is kinematically allowed by the anomalous dispersion of the phonon mode [i.e.,

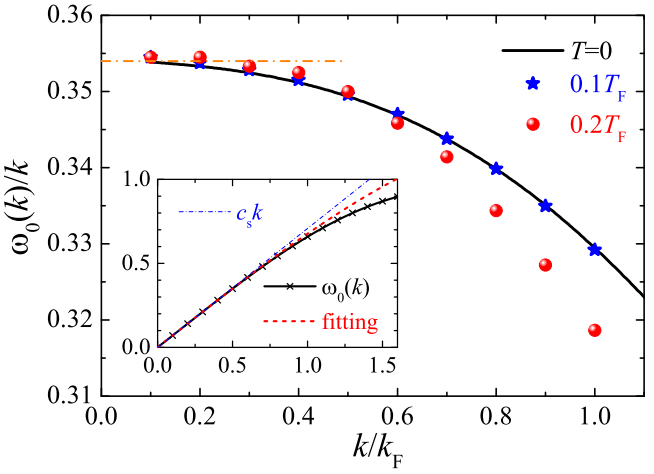

FIG. 4. The phonon phase velocity $\omega_0(k)/k$ of a unitary Fermi gas at three different temperatures, as indicated. The horizontal orange dotted-dashed line indicates the sound velocity at zero temperature $c_s = (\xi/3)^{1/2} v_F \simeq 0.354 v_F$. The inset presents the zero-temperature dispersion relation $\omega_0(k)$, together with the leading-order contribution $\omega_0(k) \simeq c_s k$ (blue dotted-dashed line). The red dashed line is the fitting curve that takes into account the next order, i.e., $\omega_0(k) \simeq c_s k(1 + \zeta k^2)$, where $\zeta = -0.044(3) k_F^{-2} < 0$.

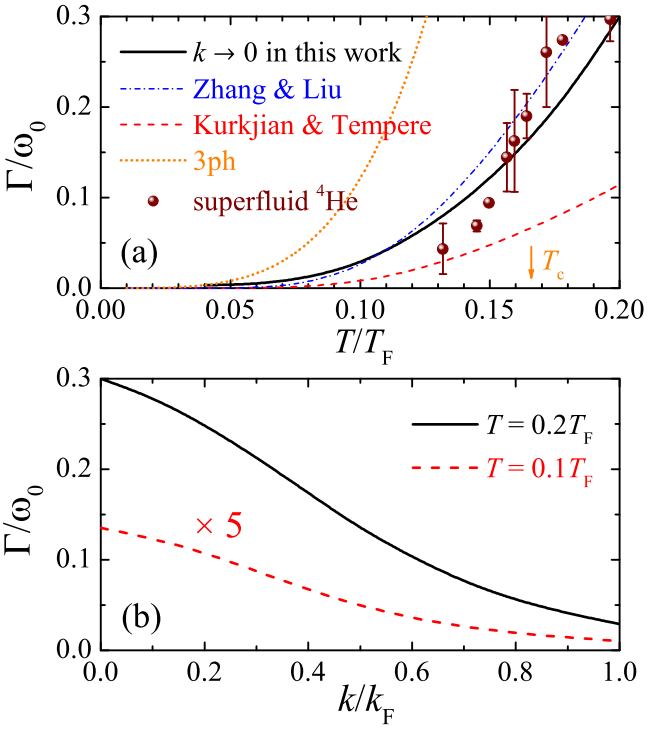

FIG. 5. (a) Temperature dependence of the inverse quality factor Γ/ω_0 of a unitary Fermi gas at $k \to 0$ (black solid line). For comparison, we show the results by Zhang and Liu (blue dotted-dashed line) [32,52] and by Kurkjian and Tempere (red dashed line) [34,53], due to scatterings off fermionic quasiparticles, and the prediction Eq. (5) by Kurkjian, Castin, and Sinatra due to the three-phonon interaction process (orange dotted line) [31], all of which are applicable in the limit of small momentum $k \to 0$. We show also Γ/ω_0 of superfluid ^{4}He at $k = 0.4$ Å^{-1} and at saturated vapor pressure (circles) [54], with temperature rescaled as $T \to (T/T_c^{\mathrm{He}}) \times T_c$. The arrow indicates the transition temperature of a unitary Fermi gas $T_c \simeq 0.167 T_F$. (b) The inverse quality factor Γ/ω_0 of a unitary Fermi gas at two temperatures $T = 0.1T_F$ and $T = 0.2T_F$, as a function of the transferred momentum. The result at $T = 0.1T_F$ has been amplified by a factor of 5 for better visualization. As predicted earlier [34], the inverse quality factor Γ/ω_0 decreases steadily with increasing transferred momentum k. At large momentum, the suppression of the damping rate can be understood from the reduced phase space due to momentum and energy conservation requirements in the inelastic scatterings.

$\omega_0(k) = c_s k(1 + \zeta k^2)$ with a positive $\zeta > 0$] at $k < k_c \sim 0.55$ Å^{-1}. The much weaker four-phonon process is possible at $k > k_c$. For temperatures above 1 K, the last inelastic process becomes favorable by scattering from thermally excited rotons.

For a unitary Fermi gas, Kurkjian and co-workers suggested that the three-phonon process is the dominant decay mechanism, since the standard RPA theory predicts a positive ζ [50], and derived an elegant expression for the inverse quality factor at low temperature [31],

$$\frac{\Gamma}{\omega_0} \overset{k\to 0}{=} \frac{16\pi^5\sqrt{3}}{405}\xi^{3/2}\left(\frac{k_B T}{mc_s^2}\right)^4 \simeq 1.2\times 10^3\left(\frac{T}{T_F}\right)^4, \quad (5)$$

where we have used the Bertsch parameter $\xi = 0.376$ [13]. This observation, however, is not conclusive, since our more accurate SLDA-RPA theory gives a negative ζ at both zero and finite temperatures, as shown in Fig. 4. Another qualitative ϵ-expansion theory provides a similar negative ζ at unitarity [51]. On the other hand, it is known that the three-phonon process in ^{4}He is only relevant at low temperature (i.e., $T < 1.0\ \mathrm{K} \sim 0.5T_c^{\mathrm{He}}$) [2,4]. It is thus unlikely to be the main damping source in a unitary Fermi gas for $T > 0.5T_c \sim 0.09T_F$. From the above considerations, we would like to argue that the inelastic scatterings of phonons from fermionic quasiparticles causes their damping at the temperature region $T \gtrsim 0.1T_F$, which is of great experimental interest.

If this is true, we expect that the damping rate Γ will be approximately proportional to the number of fermionic quasiparticles present, i.e., $\Gamma \propto e^{-E_{\min}/k_B T}$, where $E_{\min} \equiv \min\{E(k)\}$ is the minimum energy of single particles that satisfies some momentum and energy conservation requirements to allow inelastic scatterings. An analytic expression for Γ was first derived by Zhang and Liu by considering the phase fluctuations at small momentum $k \to 0$ within the mean-field RPA [32,52]. Recently, the same mean-field treatment has been improved by Kurkjian and Tempere, who found that the amplitude fluctuations may have the same significant contributions as the phase fluctuations to the phonon damping rate [34,53]. The effect of the renormalized single-particle dispersion beyond mean field has also been considered by Castin, Sinatra, and Kurkjian most recently [33], using a phenomenological description of the interactions between quasiparticles based on quantum hydrodynamics. Although we cannot obtain an analytic expression for Γ/ω_0 in the long-wavelength limit, our SLDA-RPA theory has the advantages that (i) it starts from a fundamental microscopic description and (ii) it takes into account the modified single-particle dispersion due to the beyond mean-field effect [35,36].

The SLDA-RPA results at $k \to 0$ are reported in Fig. 5(a) using a solid line. For comparison, we show also the former two RPA predictions by Zhang *et al.* [32,52] and Kurkjian *et al.* [34,53]. Our result at small momentum qualitatively agrees with both predictions, as one may anticipate. We note that, although these two predictions are derived based on the mean-field theory, for the results shown in Fig. 5(a), we have taken the accurate chemical potential and pairing order parameter, as measured from the experiments [52,53]. It is also worth mentioning that, for a strongly interacting Fermi gas, the accuracy of any theoretical predictions can only be tested by *ab initio* quantum Monte Carlo simulations or reliable experimental measurements. As our SLDA-RPA theory has been examined to provide a quantitative account of the low-momentum dynamic structure factor of a unitary Fermi gas at low temperature, we anticipate that it also gives a reliable prediction for the phonon damping rate.

It is interesting to note that the damping rate of phonons in superfluid ^{4}He at $k = 0.4$ Å^{-1} [circles in Fig. 5(a)] [54,55] closely follows our prediction at small momentum. This similarity between superfluid ^{4}He and a unitary Fermi gas suggests that any strongly interacting quantum fluids may share a *universal* damping rate for phonons, independent of their entirely different internal structures and quantum statistics.

Conclusions. In summary, we have developed a finite-temperature microscopic theory of the density response of a unitary Fermi gas at small transferred momentum, and have quantitatively examined its reliability by comparing our theoretical results with the latest Bragg scattering measurements [20]. We have clarified that the damping rate of the Goldstone phonon mode is largely due to the inelastic scatterings from fermionic quasiparticles and have predicted its universal temperature dependence, which is to be confronted with future experimental confirmation.

Acknowledgments. We are grateful to Sascha Hoinka and Chris Vale for sharing their experimental data. Our research was supported by the National Natural Science Foundation of China, Grant No. 11747059 (P.Z.), and Australian Research Council's (ARC) Discovery Projects No. FT130100815 and No. DP170104008 (H.H.), and No. FT140100003 and No. DP180102018 (X.J.L.).

[1] P. Nozières and D. Pines, *Theory of Quantum Liquids, Volume II:Superfluid Bose Liquids* (Addison-Wesley, Redwood City, CA, 1990).
[2] A. Griffin, *Excitations in a Bose-Condensed Liquid* (Cambridge University Press, New York, 1993).
[3] I. M. Khalatnikov, *Introduction to the Theory of Superfluidity* (Benjamin, New York, 1965).
[4] A. D. B. Woods and R. A. Cowley, Rep. Prog. Phys. **36**, 1135 (1973).
[5] K. M. O' Hara, S. L. Hemmer, M. E. Gehm, S. R. Granade, and J. E. Thomas, Science **298**, 2179 (2002).
[6] M. Randeria and E. Taylor, Annu. Rev. Condens. Matter Phys. **5**, 209 (2014).
[7] I. Bloch, J. Dalibard, and W. Zwerger, Rev. Mod. Phys. **80**, 885 (2008).
[8] C. A. Regal, M. Greiner, and D. S. Jin, Phys. Rev. Lett. **92**, 040403 (2004).
[9] N. Navon, S. Nascimbène, F. Chevy, and C. Salomon, Science **328**, 729 (2010).
[10] T.-L. Ho, Phys. Rev. Lett. **92**, 090402 (2004).
[11] H. Hu, P. D. Drummond, and X.-J. Liu, Nat. Phys. **3**, 469 (2007).
[12] S. Nascimbène, N. Navon, K. J. Jiang, F. Chevy, and C. Salomon, Nature (London) **463**, 1057 (2010).
[13] M. J. Ku, A. T. Sommer, L. W. Cheuk, and M. W. Zwierlein, Science **335**, 563 (2012).
[14] L. A. Sidorenkov, M. K. Tey, R. Grimm, Y.-H. Hou, L. Pitaevskii, and S. Stringari, Nature (London) **498**, 78 (2013).
[15] X.-J. Liu and H. Hu, Phys. Rev. A **67**, 023613 (2003).
[16] J. Kinast, S. L. Hemmer, M. E. Gehm, A. Turlapov, and J. E. Thomas, Phys. Rev. Lett. **92**, 150402 (2004).
[17] M. Bartenstein, A. Altmeyer, S. Riedl, S. Jochim, C. Chin, J. H. Denschlag, and R. Grimm, Phys. Rev. Lett. **92**, 203201 (2004).
[18] H. Hu, A. Minguzzi, X.-J. Liu, and M. P. Tosi, Phys. Rev. Lett. **93**, 190403 (2004).
[19] A. Altmeyer, S. Riedl, C. Kohstall, M. J. Wright, R. Geursen, M. Bartenstein, C. Chin, J. H. Denschlag, and R. Grimm, Phys. Rev. Lett. **98**, 040401 (2007).
[20] S. Hoinka, P. Dyke, M. G. Lingham, J. J. Kinnunen, G. M. Bruun, and C. J. Vale, Nat. Phys. **13**, 943 (2017).
[21] A. Minguzzi, G. Ferrari, and Y. Castin, Eur. Phys. J. D **17**, 49 (2001).
[22] R. Combescot, M. Y. Kagan, and S. Stringari, Phys. Rev. A **74**, 042717 (2006).
[23] S. Stringari, Phys. Rev. Lett. **102**, 110406 (2009).
[24] P. Zou, E. D. Kuhnle, C. J. Vale, and H. Hu, Phys. Rev. A **82**, 061605(R) (2010).
[25] H. Guo, C.-C. Chien, and K. Levin, Phys. Rev. Lett. **105**, 120401 (2010).
[26] F. Palestini, P. Pieri, and G. C. Strinati, Phys. Rev. Lett. **108**, 080401 (2012).
[27] H. Hu and X.-J. Liu, Phys. Rev. A **85**, 023612 (2012).
[28] L. He, Ann. Phys. (NY) **373**, 470 (2016).
[29] P. Zou, F. Dalfovo, R. Sharma, X.-J. Liu, and H. Hu, New J. Phys. **18**, 113044 (2016).
[30] E. Vitali, H. Shi, M. Qin, and S. Zhang, Phys. Rev. A **96**, 061601(R) (2017).
[31] H. Kurkjian, Y. Castin, and A. Sinatra, Ann. Phys. (Berlin) **529**, 1600352 (2017).
[32] Z. Zhang and W. V. Liu, Phys. Rev. A **83**, 023617 (2011).
[33] Y. Castin, A. Sinatra, and H. Kurkjian, Phys. Rev. Lett. **119**, 260402 (2017).
[34] H. Kurkjian and J. Tempere, New J. Phys. **19**, 113045 (2017).
[35] Y. Yu and A. Bulgac, Phys. Rev. Lett. **90**, 222501 (2003).
[36] A. Bulgac, Phys. Rev. A **76**, 040502(R) (2007).
[37] In our numerical calculations, the cutoff momentum Λ is sent to ∞, as all the final equations are free from divergence due to renormalization.
[38] In principle, the effective mass m^* of Bogoliubov quasiparticles differs from the bare mass m of fermions. However, this

difference is very small near the unitary limit [35,36], so we set $m^* = m$ for simplicity. This simple choice also ensures that the f-sum rule of the dynamic structure factor is strictly satisfied.

[39] J. Carlson and S. Gandolfi, Phys. Rev. A **90**, 011601(R) (2014).

[40] E. D. Kuhnle, H. Hu, X.-J. Liu, P. Dyke, M. Mark, P. D. Drummond, P. Hannaford, and C. J. Vale, Phys. Rev. Lett. **105**, 070402 (2010).

[41] H. Hu, X.-J. Liu, and P. D. Drummond, Europhys. Lett. **91**, 20005 (2010).

[42] A. Brunello, F. Dalfovo, L. Pitaevskii, S. Stringari, and F. Zambelli, Phys. Rev. A **64**, 063614 (2001).

[43] P. B. Blakie, R. J. Ballagh, and C. W. Gardiner, Phys. Rev. A **65**, 033602 (2002).

[44] We note that, if we swap the order of two convolutions, the resulting spectrum remains essentially the same. The convolution operation also does not violate the f-sum rule for the density response function and dynamic structure factor.

[45] H. Hu, X.-J. Liu, and P. D. Drummond, Europhys. Lett. **74**, 574 (2006); the predicted equations of state by this Gaussian pair fluctuation theory agree excellently well with the measured equations of state at the BEC-BCS crossover at nearly zero temperature (see, for example, Fig. 3(a) in Ref. [9]).

[46] We note that the use of the latest experimental data for the chemical potential and pairing gap in the unitary limit, i.e., $\mu = 0.376(4)$ [13] and $\Delta = 0.47(3)$ [20], gives rise to very similar values of $\beta \simeq -0.451$ and $1/\gamma \simeq -0.090$.

[47] X.-J. Liu and H. Hu, Phys. Rev. A **68**, 033613 (2003).

[48] W. Zheng and H. Zhai, Phys. Rev. Lett. **113**, 265304 (2014).

[49] H. Shen and W. Zheng, Phys. Rev. A **92**, 033620 (2015).

[50] H. Kurkjian, Y. Castin, and A. Sinatra, Phys. Rev. A **93**, 013623 (2016).

[51] R. Haussmann, M. Punk, and W. Zwerger, Phys. Rev. A **80**, 063612 (2009).

[52] The analytic expression derived by Zhang and Liu takes the form [32] $\Gamma/\omega_0 = (3\pi/2)(c_s/v_F)^3(1+\Delta^2/\xi_p^2)^2 e^{-E(p)/k_BT}$, where the wave vector p satisfies $\hbar p\xi_p = mc_sE_p$ with $\xi_p \equiv \hbar^2p^2/(2m) - \mu$ and $E_p = \sqrt{\xi_p^2+\Delta^2}$. By setting $\mu = 0.376\varepsilon_F$ and $\Delta = 0.47\varepsilon_F$, we find that $p \simeq 0.784k_F$, $E(p) \simeq 0.527\varepsilon_F$, and $\Gamma/\omega_0 \simeq 5.0e^{-0.527T_F/T}$. The last expression gives the blue dotted-dashed line in Fig. 5(a).

[53] The analytic expression derived by Kurkjian and Tempere is given by [34] $\Gamma/\omega_0 = (3\pi/2)(c_s/v_F)^3[(d\Delta/d\mu)(\Delta/\xi_p) + \Delta^2/\xi_p^2]^2 e^{-E(p)/k_BT}$. It has the same form as the one derived by Zhang and Liu, except that the factor of 1 in the latter expression is replaced with $(d\Delta/d\mu)(\Delta/\xi_p)$, due to the inclusion of the amplitude fluctuations. By setting $\mu = 0.376\varepsilon_F$ and $\Delta = 0.47\varepsilon_F$, and estimating $d\Delta/d\mu \simeq -0.58$ at unitarity from the Gaussian pair fluctuation theory (GPF) theory [45], we obtain $\Gamma/\omega_0 \simeq 1.6e^{-0.527T_F/T}$, which is about three times smaller than the damping rate given by Zhang and Liu [see, i.e., the red dashed line in Fig. 5(a)].

[54] W. G. Stirling and H. R. Glyde, Phys. Rev. B **41**, 4224 (1990).

[55] If we treat the wave vector of rotons at saturated vapor pressure, $k_R = 1.925$ Å^{-1}, as the Fermi wave vector k_F^{He} for ^{4}He atoms, then the case of $k = 0.4$ Å^{-1} corresponds to $k/k_F^{\mathrm{He}} \simeq 0.2$ and may be viewed as the limit of small transferred momentum $k \to 0$.